# Structures of Carbazole−$(H_2O)_n$ ($n = 1-3$) Clusters Studied by IR Dip Spectroscopy and a Quantum Chemical Calculation

**Makoto Sakai,[†] Kota Daigoku,[‡] Shun-ichi Ishiuchi,[†] Morihisa Saeki,[†] Kenro Hashimoto,[‡] and Masaaki Fujii*,[†]**

*Institute for Molecular Science/Graduate School for Advanced Study, Okazaki 444−8585, Japan, and Computer Center & Department of Chemistry, Graduate School of Science, Tokyo Metropolitan University/ACT-JST, Hachioji 192-0397, Japan*

*Received: June 12, 2001*

The IR spectra of carbazole and carbazole−$(H_2O)_n$ ($n = 1-3$) clusters in a supersonic jet have been measured by IR dip spectroscopy. The spectra show clear vibrational structures of both the monomer and the clusters in the 2900−3800 $cm^{-1}$ frequency region. The observed vibrational bands are assigned to the NH stretch of carbazole and the OH stretches of $H_2O$ molecules in the clusters. The geometries and IR spectra of carbazole−$(H_2O)_n$ clusters were calculated at the HF/6-31G and B3LYP/6-31++G(d,p) levels. From a comparison of the observed and calculated IR spectra, the structures of the cluster have been determined.

## 1. Introduction

It is known that carbazole shows an interesting solvent dependence in photochemical reactions after two-photon excitation.[1−5] In nonpolar solvents, such as cyclohexane, the primarily product is the neutral carbazyl radical formed by the abstraction of the imino hydrogen from carbazole.[1−3] On the other hand, in polar solvents, such as acetonitrile, the main product is the cation radical.[4,5] However, neither the reaction mechanism nor the role of the solvent has yet been established. A spectroscopic study of the solvated clusters of carbazole is one of the best approaches to this intriguing problem, since it gives detailed microscopic information on the solute−solvent interaction.

Carbazole clusters solvated with rare-gas atoms,[6−10] alkyl cyanides,[11−13] water,[14,15] ammonia[15] and carbazole homo-dimer[16] in a supersonic jet have been studied by laser-induced fluorescence (LIF)[11−16] and resonant two-photon ionization (R2PI).[6−10,14,15] The vibronic structure in the $S_1-S_0$ transition and the proton transfer in $S_1$ have been discussed. Despite many efforts, the structures of the solvated clusters have not been determined experimentally, even in the ground state, $S_0$.

In this work, as a first step to understand the photochemical reaction of carbazole, we investigated the structures of carbazole−$(H_2O)_n$, ($n = 1-3$), clusters in $S_0$ by vibrational spectroscopy combined with quantum chemical calculations. The key vibrations to characterize the structures are the NH stretch in carbazole and OH stretches in the waters. Their frequencies sensitively reflect the hydrogen bonds in solvated clusters. We observed the NH stretch vibrations of carbazole and the OH stretches of waters in the clusters by IR dip spectroscopy, which measures IR transitions of a specific cluster by the depletion of the $S_1-S_0$ resonant enhanced multiphoton ionization signal. This ion-detected IR dip spectroscopy has the advantage of selecting the molecular species not only by the mass, but also by the electronic transition. The IR bands and the cluster geometries were analyzed using quantum chemical calculations at the HF/6-31G and the B3LYP/6-31++G(d,p) levels. From a comparison between the observed and calculated IR spectra, the structures of the clusters can be determined. The hydration structure has been compared to that of indole.[17−23]

## 2. Experiments

**2.1. Ion-Detected IR Dip Spectroscopy.** The IR spectra of carbazole−$(H_2O)_n$ ($n = 0-3$) clusters are measured by IR dip spectroscopy.[24−27] This method has been used for the vibrational spectroscopy of jet-cooled molecules[25−28] and neutral[22−27,29−46] and ionic clusters.[21,47−54] The IR laser ($\nu_{IR}$) irradiates the sample molecule in a supersonic jet and is scanned in the energy region from 2900 to 3800 $cm^{-1}$. The UV laser ($\nu_{UV}$) ionizes the molecules in the ground vibrational state by resonant-enhanced two-photon ionization via the $S_1$ state. When the frequency of the IR laser matches the transition to a certain vibrationally excited state, the ion current decreases due to the loss of population from the ground state. Thus, the vibrational transition in $S_0$ can be detected as a depletion of the ion current (ion-detected IR dip spectroscopy). Each IR dip spectrum of the carbazole monomer and carbazole−$(H_2O)_n$ ($n = 1-3$) clusters was obtained by monitoring the ion current of the selected ion with a mass filter.

The details of the apparatus for ion-detected IR dip spectroscopy are presented elsewhere.[55−57] The same experimental setup was used to measure the IR−UV hole-burning spectrum. Briefly, the second harmonic of the $Nd^{3+}$:YAG laser (Powerlite 8010) and the output of a dye laser (Lumonics HD-500) pumped by the second harmonic of the $Nd^{3+}$:YAG laser were differentially mixed in a $LiNbO_3$ crystal to generate tunable IR. The typical IR laser power at the 3 $\mu$m region is 0.3 mJ. It should be noted that the IR laser intensity is very weak in the region from 3455 to 3515 $cm^{-1}$, because of the color center absorption in the $LiNbO_3$ crystal. UV radiation was generated with a KDP crystal (Inrad, Autotracker II) by frequency-doubling of a second dye laser (Lumonics HD-500) pumped by the second harmonic of another YAG laser (Spectra Physics, GCR-170). Both IR

* To whom all correspondence should be addressed. E-mail: mfujii@ims.ac.jp.
[†] Institute for Molecular Science.
[‡] Tokyo Metropolitan University.

10.1021/jp012218t CCC: $20.00 
Published on Web 08/30/2001

and UV lasers were coaxially introduced into a vacuum chamber (Toyama/Hakuto) and crossed a supersonic jet. The IR laser irradiated the sample prior to the UV laser pulse by ~50 ns. A decrease in the ground-state population caused by the IR excitation was monitored through ionization by UV light fixed at a vibronic band of the clusters. The pulsed valve and the UV laser were operated at 20 Hz, while the IR laser was synchronized to half the repetition rate. Thus, every other UV pulse provided an ionization signal with or without IR excitation. Shot-to-shot subtraction from the IR−ON signal by the IR−OFF signal greatly reduced the long-term fluctuation in the ion-detected IR spectrum. The free carbazole or hydrated carbazoles ionized by using the UV laser were detected by a channel multiplier (Murata Ceratron) through a quadrupole mass filter (Extrel). The signal was amplified by a preamplifier (EG&G PARC model 115) and integrated by a digital boxcar (EG&G PARC model 4420/4422). The integrated signal was recorded by a personal computer (NEC PC 9801) as a function of the IR laser frequency.

The carbazole−$(H_2O)_n$ ($n = 0-3$) clusters were generated by a supersonic expansion from a pulsed solenoid valve with a 0.8 mm orifice. The solid carbazole sample was placed in a small holder, which was directly attached to the valve. Both the sample holder and the valve were heated to 423 K by a sheath heater. Helium carrier gas, containing water vapor at 278 K after passing through a reservoir, was flowed into the sample holder for mixing with the carbazole vapor and pulsed out into the chamber at a 20 Hz repetition rate. The typical stagnation pressure was 2 atm, and the pressure inside the chamber was kept at $\leq 10^{-5}$ Torr during the measurements.

**2.2. Computational Method.** The molecular structures of carbazole−$(H_2O)_n$ ($n = 0-3$) were optimized by the energy-gradient technique at first by the HF/6-31G method.[58] The harmonic frequencies of each optimized structure were calculated by using the analytic second-derivative matrix along the nuclear coordinates. If the optimized structure, often obtained under some symmetry constraint, had one or more imaginary frequencies, we further optimized the structure until the true local minimum was obtained, where all of the vibrational frequencies were real. In addition, the geometrical parameters of the low-energy structures for each $n$ obtained by this procedure were refined at the B3LYP level[59−61] with the 6-31++G(d,p) basis sets. Vibrational analyses were again carried out to confirm the minima on the potential-energy surface. The IR intensities of each vibration were evaluated for all minimum structures at both the HF and B3LYP levels. The total binding energies, including a zero-point vibrational correction (ZPC), were computed by using scaled harmonic frequencies. The scale factor, 0.957 (0.905), was determined by the average ratio between the experimental and the B3LYP-(HF)-calculated frequencies of three fundamental vibrations: the NH stretch of a carbazole monomer and the symmetric $\nu_1$ and antisymmetric $\nu_3$ OH stretches of a free water molecule. The basis set superposition errors for the total binding energies at the B3LYP level were corrected by the counterpoise correction (CPC). The program used was Gaussian 98.[62]

## 3. Results and Discussion

**3.1. IR Dip Spectra of Carbazole and Carbazole−$(H_2O)_n$ Clusters.** Figure 1a shows the ion-detected IR dip spectrum of the carbazole monomer obtained when the UV laser was fixed to its $S_1$ origin (30810 $cm^{-1}$).[14] One strong band was observed at 3517 $cm^{-1}$, and we assigned it to the NH stretching vibration ($\nu_{NH}$) from its frequency. The IR dip spectra of carbazole−$(H_2O)_n$ ($n = 1-3$) clusters are shown in Figure 1b−d. They were obtained by fixing the UV laser to the $S_1$ origin of each species: 30 317, 30 077, and 30 006 $cm^{-1}$ for carbazole−$(H_2O)_n$ ($n = 1-3$), respectively.[14]

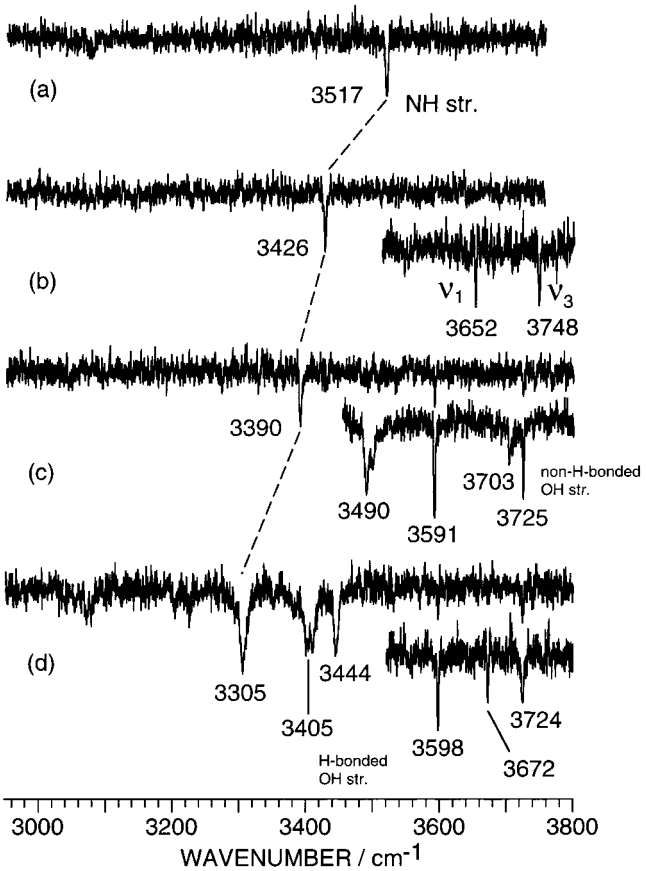


**Figure 1.** Ion-detected IR dip spectra of carbazole and carbazole−$(H_2O)_n$ ($n = 1-3$) clusters. Spectra in the 3500−3800 $cm^{-1}$ energy region were obtained by increasing the IR laser intensity.

The IR dip spectrum for the 1:1 complex (Figure 1b) shows three bands at 3426, 3652, and 3748 $cm^{-1}$. Two higher bands are assignable to the $\nu_3$ (3748 $cm^{-1}$) and $\nu_1$ (3652 $cm^{-1}$) modes of the water from their positions. Thus, the third band is assigned to $\nu_{NH}$. The $\nu_{NH}$ is red shifted by 91 $cm^{-1}$ from that of bare carbazole, while the water bands are shifted only slightly from the corresponding frequency in an isolated water molecule.[63] The water molecule is expected to be bound to NH from the O side having two free OH bonds in the cluster. It should be noted that the intensity of the IR laser decreases from ca. 3600 $cm^{-1}$ to higher because of the color center absorption (see experimental). Thus, the true absorption intensity of the water $\nu_3$ band is much higher than that of $\nu_1$, as mentioned later in detail.

Parts c and d of Figure 1 show the IR dip spectra of carbazole−$(H_2O)_2$ and carbazole−$(H_2O)_3$, respectively. The lowest band is tentatively assigned to $\nu_{NH}$ of carbazole in each cluster. The bands around 3700 $cm^{-1}$ are assigned to the stretching vibrations of free OH bonds in the cluster (non-H-bonded $\nu_{OH}$). Consequently, the bands between $\nu_{NH}$ and the non-H-bonded OH stretches are assigned to the stretching vibrations of the H-bonded OH groups of the water moieties (H-bonded $\nu_{OH}$). The two lowest bands are further red-shifted from $n = 2$, while the frequencies of the three higher bands are almost unchanged by the addition of the third water.

In Figure 1a−d, weak bands can also be found in the region of 3000−3200 $cm^{-1}$. From their frequencies, they are assigned to CH stretching vibrations of carbazole in the cluster.

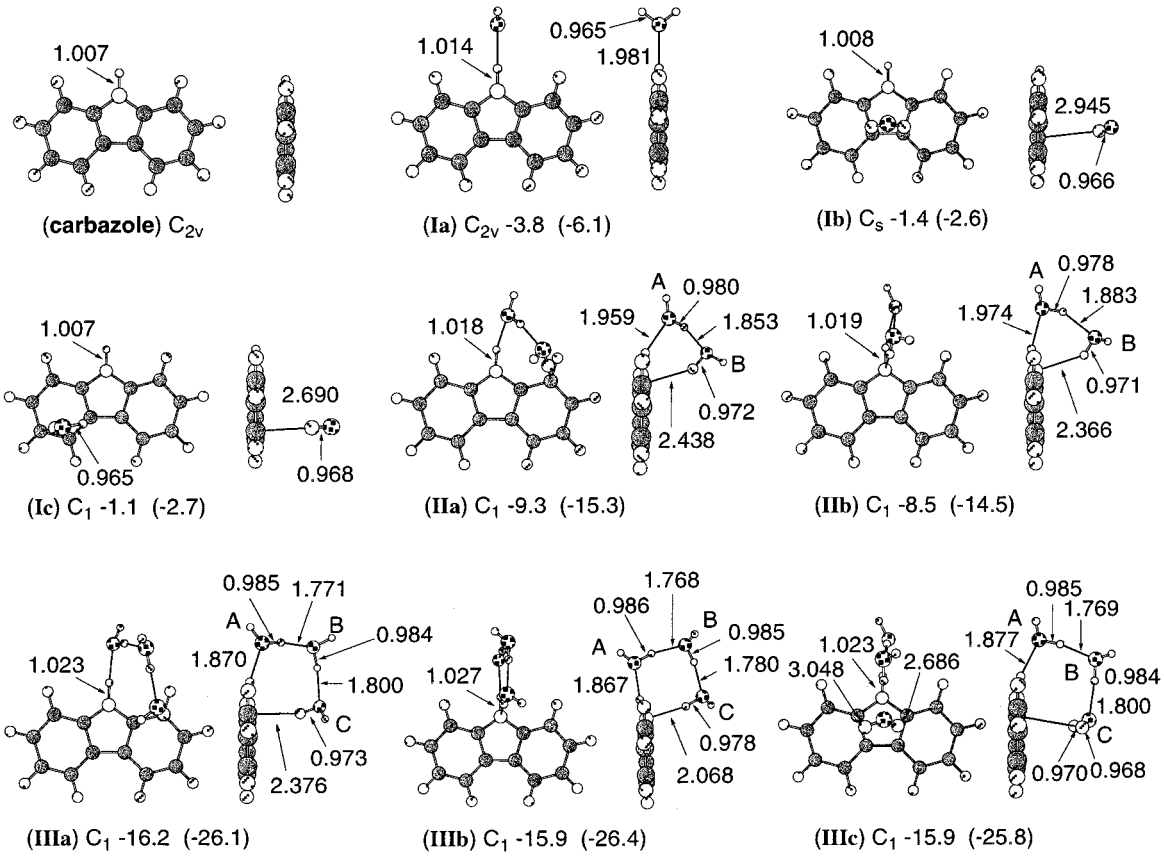


**Figure 2.** Optimized geometries of carbazole−$(H_2O)_n$ ($n = 0-3$) at the B3LYP/6-31++G(d,p) level. Molecular symmetry and total binding energies (kcal/mol) with zero-point vibrational correction (ZPC) and counterpoise correction (CPC) are presented. Values in parentheses are total binding energies (kcal/mol) without ZPC and CPC. NH, OH, and hydrogen bond distances are given in angstroms.

**3.2. Optimized Structures and Comparison of the Observed and Calculated Spectra.** The optimized geometries of carbazole−$(H_2O)_n$ ($n = 0-3$) at the B3LYP/6-31++G(d,p) level are shown in Figure 2 together with the total binding energies. The calculated NH and OH stretch frequencies of the clusters and those of free carbazole and water molecules are listed in Table 1 together with the experimental values.

The carbazole monomer is a $C_{2v}$ structure whose NH length and scaled $\nu_{NH}$ frequency are calculated to be 1.007 Å and 3523 $cm^{-1}$, respectively. For the 1:1 complex, we obtained three structures. One is a structure where carbazole donates NH to the hydrogen bond and both OH bonds are free. In other isomers, the water molecule is located on one of the carbon rings. **Ia** is lower in energy than **Ib** and **Ic** by 4 kcal/mol, indicating that this complex is more abundant than others in a supersonic jet.

The calculated IR spectra for **Ia**−**c** are compared with the observed one for $n = 1$ in Figure 3. Clearly, **Ia** reproduces the three observed bands much better than two other isomers. The scaled calculated frequencies of the bands for **Ia** are 3410, 3648, and 3761 $cm^{-1}$. The red shift of the lowest band from $n = 0$ to $n = 1$ reflects an elongation of the NH bond due to hydrogen-bond formation. The calculated relative IR intensities of the three bands are 1.00, 0.04, and 0.18. Though two higher bands seem to be equally intense in the observed spectrum, because of the rapid decrease of the IR laser power at near 3700 $cm^{-1}$, the corrected intensity of the band observed at 3748 $cm^{-1}$ is about 4.5 times greater than that at 3652 $cm^{-1}$, which is close to the calculated intensity ratio for **Ia**. Therefore, we can attribute the observed spectrum to structure **Ia** where carbazole is a proton donor.

For the carbazole−$(H_2O)_2$ cluster, we obtained six structures by the HF/6-31G method. All optimized structures for $n = 2$ and their total binding energies, as well as the calculated IR spectra at this level, are given in the Supporting Information. Three structures in which the second water molecule is bound to **Ib** or **Ic** are less stable than the other structures by over 5 kcal/mol, and none of the high-energy isomers have an intense band around 3400 $cm^{-1}$. Thus, we narrowed our focus on the three most stable forms and examined their geometries and energetics at the B3LYP/6-31++G(d,p) level. They can be regarded as complexes where the second water is hydrogen-bonded to **Ia**. Among them, the isomer in which both OH bonds in the second $H_2O$ are free from a $\pi$-hydrogen interaction had an imaginary frequency, and further optimization following the normal mode for the imaginary frequency reached **IIa**. Therefore, we finally obtained the two lowest energy structures (**IIa** and **IIb**) at the B3LYP/6-31++G(d,p) level. The second water molecule points one OH bond to the number one carbon or nitrogen atom, respectively. **IIa** is more stable than **IIb**, though the energy difference is less than 1 kcal/mol. Note that the water "bridge" in **IIa** is very similar to that in indole−$(H_2O)_2$,[22,23] where a water dimer forms a bridge from N−H to the benzene $\pi$ ring.

The calculated IR spectra of the **IIa** and **IIb** are shown in Figure 4, together with the observed IR dip spectrum for carbazole−$(H_2O)_2$. The intensity of the second lowest band is accidentally lowered due to the weak IR laser power by the color center absorption of a $LiNbO_3$ crystal. Both **IIa** and **IIb** show five bands that correspond well to the observed ones. In addition, the spectral features of the two isomers resemble each other. Thus, though it is difficult to definitely determine the orientation of the OH bond(s) in the second water, we can attribute the observed spectrum to the "bridge" structure. The two highest bands at 3730 (3731) and 3720 (3725) $cm^{-1}$ in **IIa**

**TABLE 1: Frequencies of the NH and OH Stretches in the Carbazole−$(H_2O)_n$ Clusters**

| | frequency ($cm^{-1}$) | | |
|---|---|---|---|
| | exp | calcd[a] | assignment[c] |
| $H_2O$ | 3657[b] | 3642 | $\nu_1$ |
| | 3756[b] | 3760 | $\nu_3$ |
| carbazole | 3517 | 3523 | NH str |
| carbazole−$(H_2O)_1$ | | | |
| Ia | 3426 | 3410 | NH str |
| | 3652 | 3648 | $\nu_1$ |
| | 3748 | 3761 | $\nu_3$ |
| Ib | | 3520 | NH str |
| | | 3637 | $\nu_1$ |
| | | 3738 | $\nu_3$ |
| Ic | | 3521 | NH str |
| | | 3621 | $\nu_1$ |
| | | 3734 | $\nu_3$ |
| carbazole−$(H_2O)_2$ | | | |
| IIa | 3390 | 3349 | NH str |
| | 3490 | 3430 | H-bonded OH str (A) |
| | 3591 | 3571 | $\pi$ H-bonded OH str (B) |
| | 3703 | 3720 | non-H-bonded OH str(B) |
| | 3725 | 3730 | non-H-bonded OH str (A) |
| IIb | | 3332 | NH str |
| | | 3459 | H-bonded OH str (A) |
| | | 3584 | $\pi$ H-bonded OH str (B) |
| | | 3725 | non-H-bonded OH str (B) |
| | | 3731 | non-H-bonded OH str (A) |
| carbazole−$(H_2O)_3$ | | | |
| IIIa | 3305 | 3250 | NH str + in-phase H-bonded OH str (A, B) |
| | 3405 | 3325 | in-phase H-bonded OH str (A, B) −NH str |
| | 3444 | 3375 | out-of-phase H-bonded OH str (A,B) |
| | 3598 | 3550 | $\pi$ H-bonded OH str (A, B) |
| | 3672 | 3708 | non-H-bonded OH str (C) |
| | 3724 | 3723 | non-H-bonded OH str (A) |
| | | 3725 | non-H-bonded OH str (B) |
| IIIb | | 3206 | NH str + in-phase H-bonded OH str (A, B) |
| | | 3295 | in-phase H-bonded OH str (A, B) −NH str |
| | | 3355 | out-of-phase H-bonded OH str (A,B) |
| | | 3464 | $\pi$H-bonded OH str |
| | | 3713 | non-H-bonded OH str (C) |
| | | 3718 | non-H-bonded OH str (B) |
| | | 3726 | non-H-bonded OH str (A) |
| IIIc | | 3254 | NH str + in-phase H-bonded OH str (A, B) |
| | | 3318 | in-phase H-bonded OH str (A, B) − NH str |
| | | 3371 | out-of-phase H-bonded OH str (A,B) |
| | | 3610 | $\pi$ H-bonded OH str |
| | | 3705 | non-H-bonded OH str (C) |
| | | 3721 | non-H-bonded OH str (B) |
| | | 3727 | non-H-bonded OH str (A) |

[a] Calculated at the B3LYP/6-31++G(d,p) level and scaled by 0.957. [b] Reference 63. [c] Labels in parentheses indicate water in the clusters (see Figure 2).

(**IIb**) are by the $\nu_3$ mode of waters A and B (see Figure 2), respectively. The bands at 3571 (3584) and 3430 (3459) $cm^{-1}$ are due to the stretch of the OH bond in the water B directed to the aromatic ring (the $\pi$ H-bonded $\nu_{OH}$), and that of the other OH in water A donated to the neighboring water (the H-bonded $\nu_{OH}$). On the other hand, the lowest band at 3349 (3332) $cm^{-1}$ is the NH stretch band.

For $n = 3$, we obtained 11 minimum structures at the HF/6-31G level. The geometries, total binding energies and calculated IR spectra are given in the Supporting Information. Here, we concentrate on the three most stable structures that reproduce the observed spectral feature better than other isomers. Their optimized geometries at the B3LYP/6-31++G(d,p) level are **IIIa**−**c** in Figure 2. Similarly to $n = 2$, these clusters can be regarded as "bridge"-like structures. A chain-like water trimer is hydrogen bonded to the carbazole's NH by an O atom in one terminal water, and another terminal water approaches to carbazole from above the aromatic ring. **IIIa**, whose total binding energy is −16.2 kcal/mol, is the most stable, though **IIIb** and **IIIc** are higher in energy than **IIIa** by only 0.3 kcal/mol.

The calculated and experimental spectra for $n = 3$ are compared in Figure 5. Structures **IIIa**−**c** have similar spectra and they reproduce the observed bands reasonably well. The three highest calculated frequencies, especially in **IIIa** and **IIIc**, seem to indicate a possible overlap of two bands, which is consistent with the observation of two dips in the non-H-bonded OH stretch region. The calculated bands at 3550 (**IIIa**), 3464 (**IIIb**), and 3610 (**IIIc**) $cm^{-1}$ are due to the stretch of the OH bond directed to the $\pi$ electron cloud. Thus, the corresponding band observed at 3598 $cm^{-1}$ is considered to be by this mode. The normal modes of the lower bands become delocalized in comparison with $n = 2$. The bands at 3375 (**IIIa**), 3355 (**IIIb**), and 3371 (**IIIc**) $cm^{-1}$ are mainly due to the out-of-phase stretches of two H-bonded OH bonds, while the in-phase combination of the H-bonded OH stretches is a main contributor to the band at 3325, 3295, and 3318 $cm^{-1}$ in **IIIa**−**IIIc**, respectively. The NH stretch also contributes to the second

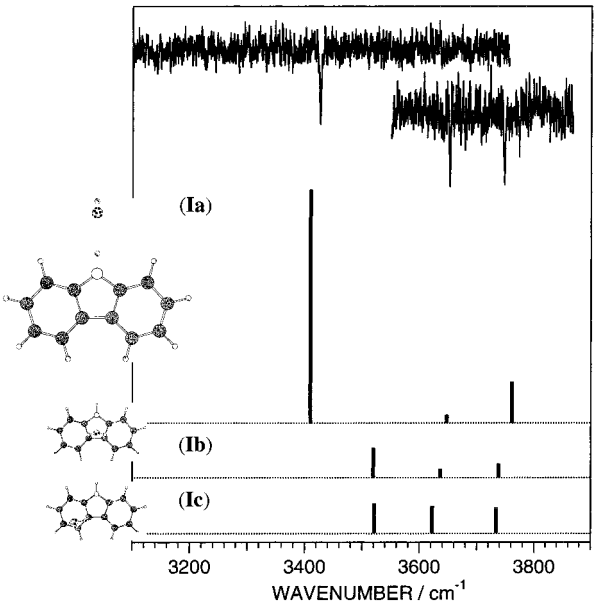


**Figure 3.** Comparison of observed and calculated spectra for $n = 1$. The cluster structures are shown as insets. The calculated frequencies are at the B3LYP/6-31++G(d,p) level and scaled by 0.957.

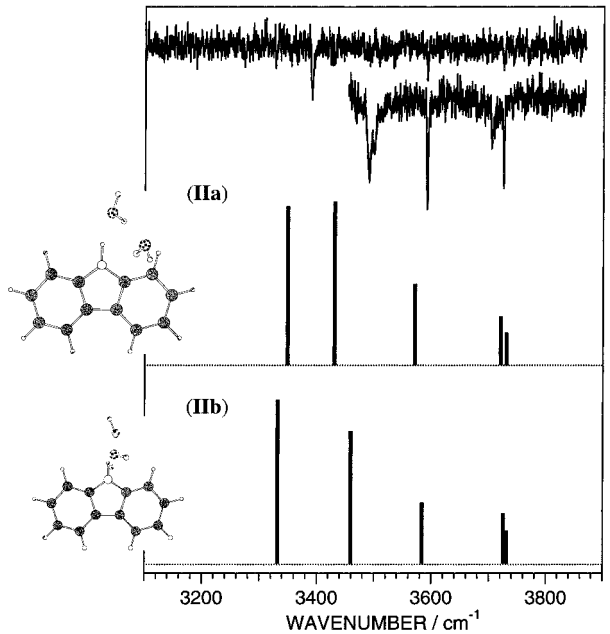


**Figure 4.** Comparison of observed and calculated spectra for $n = 2$. The cluster structures are shown as insets. The calculated frequencies are at the B3LYP/6-31++G(d,p) level and scaled by 0.957.

lowest band in each isomer, being out of phase with the H-bonded OH stretches. The lowest band can be attributed mainly to the NH stretch having the H-bonded OH bonds stretch in phase with it.

By putting the results for $n = 2$ together, we can say that the clusters with the water−chain bridging between the NH and the $\pi$ electron cloud are considered to be responsible for the observed spectra for $n = 2$ and 3. The hydration structure of carbazole is similar to that of indole with the same $n$. The frequency of the NH stretch lowers as $n$ grows. The observed bands in 3400−3500 $cm^{-1}$ are due to the H-bonded OH stretches. They indicate the number of H bonds among the waters. In addition, the bands at ca. 3600 $cm^{-1}$ can be ascribed to a $\pi$ H-bonded OH stretch of the terminal water in the water chain. Their frequencies are slightly lower than that of the water

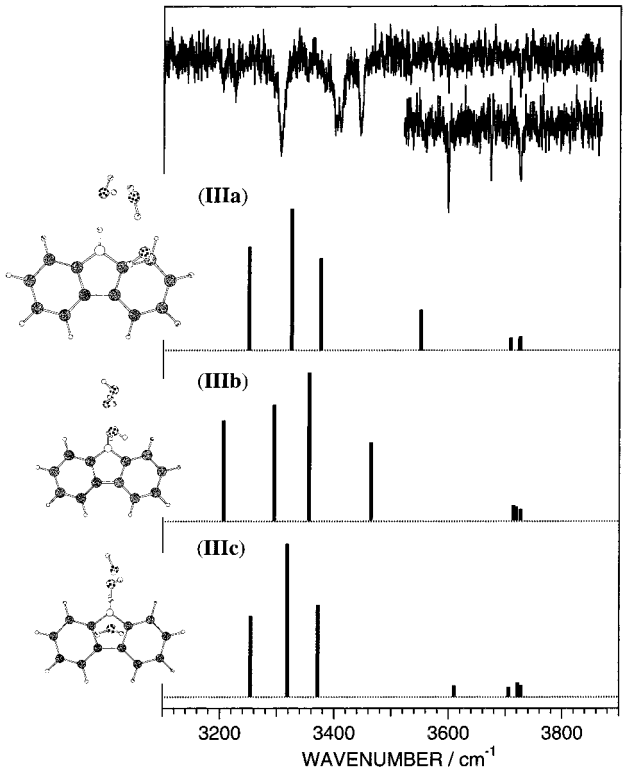


**Figure 5.** Comparison of observed and calculated spectra for $n = 3$. The cluster structures are shown as insets. The calculated frequencies are at the B3LYP/6-31++G(d,p) level and scaled by 0.957.

$\nu_1$ band, reflecting a slight elongation of the OH bonds in the $n = 2$ and 3 clusters. However, it is difficult to argue whether the bands derived form the different isomers are overlapping, which leads us to the additional experiment mentioned in the next section.

**3.3. IR−UV Hole Burning Spectra of Carbazole−$(H_2O)_{2,3}$.** To examine the coexistence of low-energy isomers, we applied IR−UV hole-burning spectroscopy to carbazole−$(H_2O)_{2,3}$. This method is a kind of population labeling spectroscopy, and has been applied to clusters to extract the electronic transitions due to a single species.[22,37−42,49] Here, the IR laser frequency is fixed to the carbazole NH stretch at 3390 and 3305 $cm^{-1}$ for carbazole−$(H_2O)_{2,3}$, respectively, while the UV laser is scanned over the energy range for the $S_1-S_0$ transition.

The UV laser is used not only for electronic excitation but also for ionization of the clusters due to resonance-enhanced two-photon ionization. If a certain $S_1$ vibronic band originates from a species whose vibration is excited by the IR laser, the ion current of the ionized cluster decreases in comparison to that without the IR laser, because of a loss of the population. Therefore, the $S_1-S_0$ electronic transition of a specific species can be identified by comparing the spectra with and without the IR laser.

Figure 6 shows the IR−UV hole-burning spectra of (a) carbazole−$(H_2O)_2$ and (b) carbazole−$(H_2O)_3$. Upper and lower traces show the spectra without and with the IR laser. In Figure 6a, all of the sharp vibronic bands disappear when an IR laser is introduced. The same result was obtained for carbazole−$(H_2O)_3$. The intensities of all the vibronic bands decrease with the IR laser (see Figure 6b). These results clearly indicate that no isomer coexists under our experimental conditions for both $n = 2$ and 3.

No observation of isomers may be understood if one considers the very low barrier for isomerization. That is, if the energy

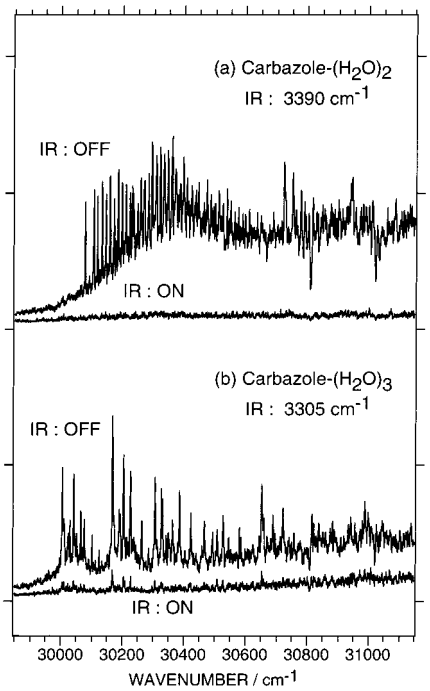


**Figure 6.** (a) $S_1 \leftarrow S_0$ mass selected (1 + 1) MPI spectra of carbazole$-(H_2O)_2$ with the IR laser and without the IR laser. The IR frequency is fixed to 3390 $cm^{-1}$. (b) $S_1 \leftarrow S_0$ mass selected (1 + 1) MPI spectra of carbazole$-(H_2O)_3$ with the IR laser and without the IR laser. The IR frequency is fixed to 3305 $cm^{-1}$.

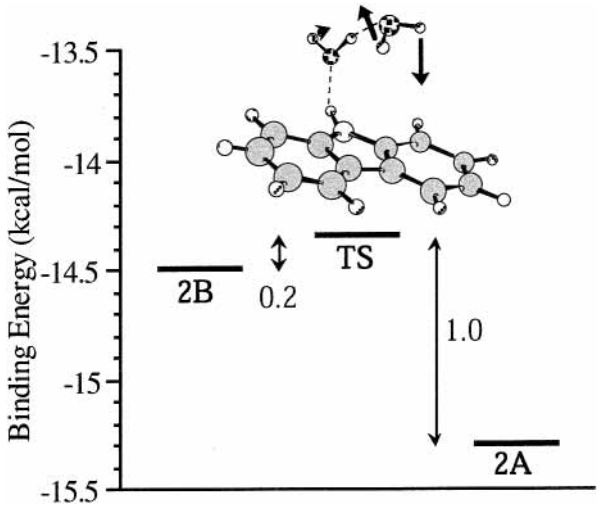


**Figure 7.** Energy diagram of IIa, IIb, and the transition state at the B3LYP/6-31++G(d,p) level. Arrows indicate the normal mode for the imaginary frequency.

barrier between **IIa** and **IIb** is so low that the ground vibrational level of the mode along the reaction coordinate is above the barrier, we expect a spectrum for a single species whose geometry and frequencies are similar to those at the global "potential minima". In fact, the transition state between **IIa** and **IIb** is located only 1.0 (0.2) kcal/mol above **IIa** (**IIb**) at the B3LYP level, and the ground vibrational level of the mode connecting **IIa** and **IIb** is 0.3 kcal/mol (with no scaling) above from the potential bottom at **IIb** within the harmonic approximation (see Figure 7).

Potential barriers connecting **IIIa**−**c** are also expected to be low, since their energies and geometries deviate little from one another. Thus, at present, we conclude that the IR dip spectra for $n = 2$ and 3 are dominated by a single "bridge" species for each $n$, and the potential energy surfaces connecting the "bridge" structures with different hydrogen orientations are very flat for both $n$.

## 4. Conclusion

The combination of ion-detected IR dip spectroscopy and quantum chemical calculations has been used to determine the structure of the aqueous clusters of carbazole. All of the IR dip spectra show clear vibrational structures due to the hydrogen-bonded NH and OH stretching modes in the clusters. The spectral features were reproduced reasonably well by the lowest energy structures for each $n = 1-3$. In the 1:1 complex, a water molecule is H-bonded to the NH group of carbazole, and the H-bonded water-chain bridges between the NH and the $\pi$ electron cloud in $n = 2$ and 3 clusters, being similar to the hydration structure of indole.

Though the present calculations show a few potential minima with the bridge structure with different water orientations, the IR−UV hole-burning measurements of carbazole$-(H_2O)_{2,3}$ have proved that only a single conformer exists in the supersonic beam for each $n = 2$ and 3. The potential energy surfaces connecting the "bridge"-like structures are very flat.

To understand the solvent dependence of the photochemical reaction, solvated clusters of carbazole with various solvents, such as methanol, acetonitrile, and cyclohexane, should be investigated by the same combination of spectroscopic technique and theoretical calculation. Also, the geometry of the photo-excited clusters is indispensable information to understand the photochemical reaction mechanism. These detailed studies will be given in a forthcoming paper.

**Acknowledgment.** The present work was financially supported in part by a Grant-in-Aid from the Ministry of Education, Science, Sports, and Culture in Japan. The support from the Daiko Foundation is also gratefully acknowledged. A part of the computations was carried out at the Computer Center at Institute for Molecular Science. We thank the IMS computer center for the allotment of computer time. K.H. is also grateful for the financial support by Research and Development Applying Advanced Computational Science and Technology, Japan Science and Technology Corp. (ACT-JST).

**Supporting Information Available:** Figures of optimized geometries of carbazole$-(H_2O)_n$ with relative energy ($n = 0-3$) and their calculated IR spectra at the HF/6-31G level (Figures 1S−6S). This material is available free of charge via the Internet at http://pubs.acs.org.

## References and Notes

(1) Yamamoto, S.; Kikuchi, K.; Kokubun, H. *Z. Phys. Chem.* **1978**, *109*, 47.
(2) Yamamoto, S.; Kikuchi, K.; Kokubun, H. *Chem. Lett.* **1977**, 1173.
(3) Martin, M.; Breheret, E.; Tfbel, F.; Lacourbas, B. *J. Phys. Chem.* **1980**, *84*, 70.
(4) Masuhara, H.; Tohgo, Y.; Mataga, N. *Chem. Lett.* **1975**, 59.
(5) Masuhara, H.; Tamai, N.; Mataga, N.; De Schryver, F. C.; Vandendriessche, J.; Boens, N. *Chem. Phys. Lett.* **1983**, *95*, 471.
(6) Bösiger, J.; Leutwyler, S. *Phys. Rev. Lett.* **1987**, *59*, 1895.
(7) Leutwyler, S.; Bösiger, J. *Chem. Rev.* **1990**, *90*, 489.
(8) Bürgi, T.; Droz, T.; Leutwyler, S. *Chem. Phys. Lett.* **1994**, *225*, 351.
(9) Droz, T.; Bürgi, T.; Leutwyler, S. *J. Chem. Phys.* **1995**, *103*, 4035.
(10) Bürgi, T.; Droz, T.; Leutwyler, S. *J. Chem. Phys.* **1995**, *103*, 7228.
(11) Auty, A. R.; Jones, A. C.; Phillips, D. *J. Chem. Soc., Faraday Trans. 2* **1986**, *82*, 1219.
(12) Taylor, A. G.; Jones, A. C.; Auty, A. R.; Phillips, D. *Chem. Phys. Lett.* **1986**, *131*, 534.

(13) Taylor, A. G.; Jones, A. C.; Phillips, D. *Chem. Phys. Lett.* **1990**, *169*, 17.
(14) Bombach, R.; Honegger, E.; Leutwyler, S. *Chem. Phys. Lett.* **1985**, *118*, 449.
(15) Honegger, E.; Bombach, R.; Leutwyler, S. *J. Chem. Phys.* **1986**, *85*, 1234.
(16) Taylor, A. G.; Jones, A. C.; Phillips, D. *Chem. Phys.* **1989**, *138*, 413.
(17) Helm, R. M.; Clara, M.; Grebner, T. L.; Neusser, H. J. *J. Phys. Chem. A* **1998**, *102*, 3268.
(18) Braun, J. E.; Grebner, T. L.; Neusser, H. J. *J. Phys. Chem. A* **1998**, *102*, 3273.
(19) Korter, T. M.; Pratt, D. W.; Küpper, J. *J. Phys. Chem. A* **1998**, *102*, 7211.
(20) Carles, S.; Desfrancois, C.; Schermann, J. P.; Smith, D. M. A.; Adamowicz, L. *J. Chem. Phys.* **2000**, *112*, 3726.
(21) Unterberg, C.; Jansen, A.; Gerhards, M. *J. Chem. Phys.* **2000**, *113*, 7945.
(22) Carney, J. R.; Hagemeister, F. C.; Zwier, T. S. *J. Chem. Phys.* **1998**, *108*, 3379.
(23) Carney, J. R.; Zwier, T. S. *J. Phys. Chem. A* **1999**, *103*, 9943.
(24) Page, R. H.; Shen, Y. R.; Lee, Y. T. *J. Chem. Phys.* **1988**, *88*, 4621. Page, R. H.; Shen, Y. R.; Lee, Y. T. *J. Chem. Phys.* **1988**, *88*, 5362.
(25) Zwier, T. S. *Annu. Rev. Phys. Chem.* **1996**, *47*, 205.
(26) Ebata, T.; Fujii, A.; Mikami, N. *Int. Rev. Phys. Chem.* **1998**, *17*, 321.
(27) Brutschy, B. *Chem. Rev.* **2000**, *100*, 3891.
(28) Tanabe, S.; Ebata, T.; Fujii, M.; Mikami, N. *Chem. Phys. Lett.* **1993**, *215*, 347.
(29) Iwasaki, A.; Fujii, A.; Watanabe, T.; Ebata, T.; Mikami, N. *J. Phys. Chem.* **1996**, *100*, 16053.
(30) Watanabe, T.; Ebata, T.; Tanabe, S.; Mikami, N. *J. Chem. Phys.* **1996**, *105*, 408.
(31) Pribble, R. N.; Zwier, T. S. *Science* **1994**, *265*, 75. Pribble, R. N.; Zwier, T. S. *Faraday Discuss.* **1994**, *97*, 229.
(32) Pribble, R. N.; Garrett, A. W.; Haber, K.; Zwier, T. S. *J. Chem. Phys.* **1995**, *103*, 531.
(33) Pribble, R. N.; Gruenloh, C.; Zwier, T. S. *Chem. Phys. Lett.* **1996**, *262*, 627.
(34) Pribble, R. N.; Hagemeister, F.; Zwier, T. S. *J. Chem. Phys.* **1997**, *106*, 2145.
(35) Gruenloh, C. J.; Florio, G. M.; Carney, J. R.; Hagemeister, F. C.; Zwier, T. S. *J. Phys. Chem. A* **1999**, *103*, 496.
(36) Gruenloh, C. J.; Hagemeister, F. C.; Carney, J. R.; Zwier, T. S. *J. Phys. Chem. A* **1999**, *103*, 503.
(37) Ebata, T. In *Population Labeling Spectroscopy*; Nonlinear Spectroscopy for Molecular Structure Determination, Vol. 6; Field, R. W., Hirota, E., Maier, J. P., Tsuchiya, S., Eds.; Blackwell Science: Oxford, U.K., 1996; pp 149−165.
(38) Matsuda, Y.; Ebata, T.; Mikami, N. *J. Chem. Phys.* **2000**, *113*, 573.
(39) Robertson, E. G.; Simons, J. P. *Phys. Chem. Chem. Phys.* **2001**, *3*, 1.
(40) Robertson, E. G.; Hockridge, M. R.; Jelfs, P. D.; Simons, J. P. *J. Phys. Chem. A* **2000**, *104*, 11714.
(41) Mons, M.; Robertson, E. G.; Simons, J. P. *J. Phys. Chem. A* **2000**, *104*, 1430.
(42) Graham, R. J.; Kroemer, R. T.; Mons, M.; Robertson, E. G.; Snoek, L. C.; Simons, J. P. *J. Phys. Chem. A* **1999**, *103*, 9706.
(43) Barth, H. D.; Buchhold, K.; Djafari, S.; Reimann, B.; Lommatzsch, U.; Brutschy, B. *Chem. Phys.* **1998**, *239*, 49.
(44) Tarakeshwar, P.; Kim, K. S.; Brutschy, B. *J. Chem. Phys.* **1999**, *110*, 8501.
(45) Tarakeshwar, P.; Kim, K. S.; Brutschy, B. *J. Chem. Phys.* **2000**, *112*, 1769.
(46) Janzen, C.; Spangenberg, D.; Roth, W.; Kleinermanns, K. *J. Chem. Phys.* **1999**, *110*, 9898.
(47) Gerhards, M.; Unterberg, C.; Kleinermanns, K. *Phys. Chem. Chem. Phys.* **2000**, *2*, 5538.
(48) Kleinermanns, K.; Janzen, C.; Spangenberg, D.; Gerhards, M. *J. Phys. Chem. A* **1999**, *103*, 5232.
(49) Fujimaki, E.; Fujii, A.; Ebata, T.; Mikami, N. *J. Chem. Phys.* **2000**, *112*, 137.
(50) Fujii, A.; Sawamura, T.; Tanabe, S.; Ebata, T.; Mikami, N. *Chem. Phys. Lett.* **1994**, *225*, 104.
(51) Nakanaga, T.; Ito, F.; Miyawaki, J.; Sugawara, K.; Takeo, H. *Chem. Phys. Lett.* **1996**, *261*, 414.
(52) Linnartz, H.; Speck, T.; Maier, J. P. *Chem. Phys. Lett.* **1998**, *288*, 504.
(53) Fujii, A.; Fujimaki, E.; Ebata, T.; Mikami, N. *J. Chem. Phys.* **2000**, *112*, 6275.
(54) Fuke, K.; Hashimoto, K.; Iwata, S. In *Structures, Spectroscopies, and Reactions of Atomic Ions with Water Clusters*; Advance in Chemical Physics, Vol. 110; Prigogine, I., Rice, S. A., Eds.; John Wiley & Sons: New York, 1999; pp 431−523.
(55) Omi, T.; Shitomi, H.; Sekiya, N.; Takazawa, K.; Fujii, M. *Chem. Phys. Lett.* **1996**, *252*, 287.
(56) Yoshino, R.; Hashimoto, K.; Omi, T.; Ishiuchi, S.; Fujii, M. *J. Phys. Chem. A* **1998**, *102*, 6227.
(57) Ishiuchi, S.; Saeki, M.; Sakai, M.; Fujii, M. *Chem. Phys. Lett.* **2000**, *322*, 27.
(58) Hehre, W. J.; Radom, L.; Schleyer, P. V. R.; Pople, J. A. *Ab initio Molecular Orbital Theory*; Wiley: New York, 1986.
(59) Becke, A. D. *J. Chem. Phys.* **1993**, *98*, 5648.
(60) Vosko, S. H.; Wilk, L.; Nusair, M. *Can. J. Phys.* **1980**, *58*, 1200.
(61) Lee, C.; Yang, W.; Parr, R. G. *Phys. Rev.* **1988**, *B37*, 785.
(62) (a) Frisch, M. J.; Trucks, G. W.; Schlegel, H. B.; Scuseria, G. E.; Robb, M. A.; Cheeseman, J. R.; Zakrzewski, V. G.; Montgomery, J. A., Jr.; Stratmann, R. E.; Burant, J. C.; Dapprich, S.; Millam, J. M.; Daniels, A. D.; Kudin, K. N.; Strain, M. C.; Farkas, O.; Tomasi, J.; Barone, V.; Cossi, M.; Cammi, R.; Mennucci, B.; Pomelli, C.; Adamo, C.; Clifford, S.; Ochterski, J.; Petersson, G. A.; Ayala, P. Y.; Cui, Q.; Morokuma, K.; Malick, D. K.; Rabuck, A. D.; Raghavachari, K.; Foresman, J. B.; Cioslowski, J.; Ortiz, J. V.; Stefanov, B. B.; Liu, G.; Liashenko, A.; Piskorz, P.; Komaromi, I.; Gomperts, R.; Martin, R. L.; Fox, D. J.; Keith, T.; Al-Laham, M. A.; Peng, C. Y.; Nanayakkara, A.; Gonzalez, C.; Challacombe, M.; Gill, P. M. W.; Johnson, B.; Chen, W.; Wong, M. W.; Andres, J. L.; Gonzalez, C.; Head-Gordon, M.; Replogle, E. S.; Pople, J. A. *Gaussian 98*, revision A.5; Gaussian, Inc.: Pittsburgh, PA, 1998. (b) Frisch, M. J.; Trucks, G. W.; Schlegel, H. B.; Scuseria, G. E.; Robb, M. A.; Cheeseman, J. R.; Zakrzewski, V. G.; Montgomery, J. A., Jr.; Stratmann, R. E.; Burant, J. C.; Dapprich, S.; Millam, J. M.; Daniels, A. D.; Kudin, K. N.; Strain, M. C.; Farkas, O. Tomasi, J.; Barone, V.; Cossi, M.; Cammi, R.; Mennucci, B.; Pomelli, C.; Adamo, C.; Clifford, S.; Ochterski, J.; Petersson, G. A.; Ayala, P. Y.; Cui, Q.; Morokuma, K.; Malick, D. K.; Rabuck, A. D.; Raghavachari, K.; Foresman, J. B.; Cioslowski, J.; Ortiz, J. V.; Baboul, A. G.; Stefanov, B. B.; Liu, G.; Liashenko, A.; Piskorz, P.; Komaromi, I.; Gomperts, R.; Martin, R. L.; Fox, D. J.; Keith, T.; Al-Laham, M. A.; Peng, C. Y.; Nanayakkara, A.; Challacombe, M.; Gill, P. M. W.; Johnson, B.; Chen, W.; Wong, M. W.; Andres, J. L.; Gonzalez, C.; Head-Gordon, M.; Replogle, E. S.; Pople, J. A. *Gaussian 98*, revision A.9; Gaussian, Inc.: Pittsburgh, PA, 1998.
(63) Fraud, J. M.; Camy-Peret, C.; Maillard, J. P. *Mol. Phys.* **1976**, *32*, 499.